

# Traveling Wave Based Protection Scheme for Inverter Dominated Microgrid Using Mathematical Morphology

X. Li, A. Dyško, *Member, IEEE*, and G. Burt, *Member, IEEE*

**Abstract**— Inverter dominated microgrids impose significant challenges on the distribution network, as inverters are well known for their limited contribution to fault current, undermining the performance of traditional overcurrent protection schemes. This paper introduces a new protection scheme based on the initial current traveling wave utilizing an improved mathematical morphology (MM) technology, with simplified polarity detection and new logics introduced for meshed networks and feeders with single-end measurement. The proposed protection scheme provides ultra-fast response and can be adapted to varied system operational modes, topologies, fault conditions and load conditions. Only low bandwidth communication is required to achieve high speed operation and adequate discrimination level in meshed networks. Simulation in PSCAD/EMTDC verifies both the sensitivity and stability of the proposed protection scheme under different microgrid operational scenarios.

**Index Terms**—Microgrid protection, initial current traveling wave, inverter dominated microgrid, mathematical morphology.

## I. INTRODUCTION

THE protection of a microgrid is often a challenge. Unlike in the conventional distribution system, protection of the microgrid needs to adapt itself to different modes of operation: mainly islanded and grid-connected regimes. It is expected to offer good sensitivity and selectivity for faults in both situations. The operation of the protection system also needs to be fast in order to protect the sensitive loads and power sources. For islanded inverter-dominated microgrids, the low fault current level usually makes the application of traditional overcurrent principles prohibitive [1]. In [2] the authors emphasize that protection of the inverter-dominated microgrids is a major challenge calling for research into new protection principles. Based on this statement, Fig. 1 gives an outline of the major protection principles which can potentially serve the inverter-dominated microgrid. These protection solutions can be seen as largely independent of the fault to load current ratio.

Xinyao Li is a PhD candidate at Electrical and Electronic Engineering Department, University of Strathclyde (Email: [xinyao.li@strath.ac.uk](mailto:xinyao.li@strath.ac.uk)).

Dr. Adam Dyško is with Electrical and Electronic Engineering Department, University of Strathclyde (Email: [a.dysko@strath.ac.uk](mailto:a.dysko@strath.ac.uk))

Prof. Graeme M. Burt is with Electrical and Electronic Engineering Department, University of Strathclyde (Email: [g.burt@eee.strath.ac.uk](mailto:g.burt@eee.strath.ac.uk))

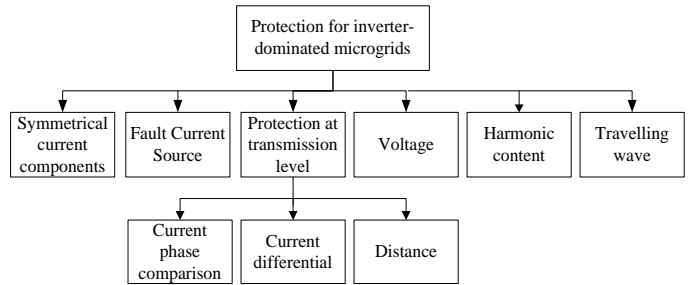


Fig. 1. Review of protection schemes for inverter-dominated microgrids

Nikkhajoei & Lasseter et al. [3] assume a protection scheme based on modified current signals such as symmetrical or differential current components. Similar to overcurrent principles, the coordination of this scheme is still based on the time grading of the current components. Time delay can be more than 10-cycles and the performance might be problematic in a meshed microgrid. Moreover, it can only detect unbalanced faults.

Van Overbeeke et al. [4] propose a dedicated Fault Current Source (FCS) offering sufficient fault current into the islanded microgrid to guarantee fault detection. Nevertheless, it can be viewed as unreliable from a protection reliability point of view, as the whole protection system relies on a single electrical device. Following this idea, in practice, most of the running microgrids are still equipped with large storage units which can provide sufficient fault current into the network [5].

Voltage [6] and harmonic content [7] based methods are two special solutions proposed by Al-Nasseri. The voltage based method makes use of the voltage level gradient through the network during faults, which implies its application in a relatively large network. Furthermore, it cannot deal with the high impedance faults (HIF). The voltage based method is, therefore, mostly recommended to act as a back-up scheme [8]. On the other hand, the harmonic content based method is mainly designed to protect the distributed generator (DG) rather than the network. Additionally, the operating threshold of the harmonic content based method is difficult to define.

There is a group of methods which are based on transmission system type protection schemes. References [9-11] apply current differential protection schemes for the inverter dominated microgrid. Halabi et al [1] present a current phase comparison scheme. These methods are all based on the assumption that a high bandwidth communication channel is

available. Devadasa et al [12] investigate the application of distance protection scheme, however no discussion or systematic simulation is included to prove its effectiveness.

Very few papers have discussed the idea of using fault generated traveling wave as a guiding principle of the microgrid protection. David et al [13] apply this idea to a zonal DC marine system. However, with no dedicated signal analysis, fault transients are not properly extracted, and their arrival time and polarity information are vague. Furthermore, the method requires very high communication bandwidth to transport high frequency sampled real time current measurements. Shi et al [14] propose a hybrid protection idea using fault generated current traveling wave and superimposed power frequency voltage using multi-resolution wavelet analysis. However, the method is not validated through any simulation or experiments.

Previous work by the authors [15] introduces a hybrid approach consisting of the main protection based on traveling wave measurements and supplemental protection based on the rate of change of current. The traveling waves are extracted by mathematical morphology filters (MMF). MMF only contains addition and subtraction which is inherently light on computing burden. Therefore, this protection is ultra-fast and can detect faults within several micro seconds. The dead zone dealing with low inception angle faults, which is the main shortcoming of all traveling wave based methods, is addressed by the supplemental protection scheme based on the rate of change of current. However, the method is limited to certain network applications as it is not fully discriminative in meshed networks and in networks where single-end measurement is used.

To address these challenges, this paper introduces additional protection logic elements and proposes a modification of the MMF which is developed using the apparent features of dilation and erosion signals. This modification delivers faster, clearer and more accurate polarity detection than the existing methods. The proposed approach is different from other MMF based protection methods, as the scheme uses polarity information from both ends of the circuit, and thus, avoids the difficulty of detecting a series of wavefronts in a distribution system [16, 29]. In order to verify the sensitivity and stability of the proposed protection scheme, a number of testing scenarios are considered including various fault conditions, system topology, system operation, sampling frequency, and signal noise. Extensive simulation studies are conducted in PSCAD/EMTDC, using the 20kV microgrid benchmark model [1]. The results show that the proposed scheme is able to protect the inverter dominated microgrid rapidly and reliably. It needs to be emphasized that the method can reliably protect microgrids incorporating other types of distributed sources (e.g. synchronous generators), since it is purely based on the fault generated transients.

This paper is organized as follows: Section II presents the algorithm of the modified MMF; Section III addresses the underlying protective principles and application; Section IV gives a detailed performance analysis of sensitivity and selectivity of the protection scheme. The discussion on the potential hardware implementation and final conclusions are presented in Sections V and VI.

## II. BASIC PRINCIPLE AND FILTER DESIGN

### A. Algorithm for signal analysis and modified MMF

The magnitude of the fault generated high frequency transients is affected by the fault inception angle, fault resistance and distance to fault. Therefore, the waveform magnitude is generally not a suitable indicator of the fault condition. By contrast, the time and polarity information provide good fault indication, and have been widely used in traveling wave based methods [16-17]. Therefore, it can be considered that the optimal signal processing tool for traveling wave based protection should present good performance for both polarity detection and time location.

The present main stream signal processing tools include Windowed Fourier Transform (WFT), Discrete Wavelet Transform (DWT) and Mathematical Morphology (MM).

Using WFT, the processed signals can only be analyzed at one definite frequency. This assumes that the signal is stationary during an observation period. For the fault transients producing non-stationary signals with large frequency spectrum, this technique is unsatisfactory [18]. By contrast, with a suitable mother wavelet, DWT can be applied as a flexible and effective bandpass filter [19-20], which uses short windows at high frequencies and long windows at low frequencies. Protection based on DWT analysis has drawn a lot of attention among researchers [21-24]. However, the high calculation burden currently makes this methodology prohibitive in the protection field. Moreover, DWT has additional shortcomings, such as poor directionality (polarity detection), shift sensitivity and oscillations around singularities [25].

An alternative method uses a nonlinear approach based on Mathematical Morphology (MM) [16]. This technique has been proved to be light on memory requirements, efficient and accurate in extracting the high frequency traveling wave information. MM uses a structural element (SE) to extract the necessary features of the original signals [16, 26-28]. The shape of SE can be flat, semi-circular, triangular, etc., which should be selected according to the shape of the anticipated transients. Dilation ( $\oplus$ ) and erosion ( $\ominus$ ) are two basic operations in MM. More details on fundamental MM theory can be found in [28].

Assuming a signal  $f(n)$  ( $0 < n < N$ ) to be analyzed, an SE  $g(m)$  ( $0 < m < M$ ) is applied to perform the signal dilation and erosion, as defined in (1) and (2) respectively.  $N$  represents the length of the moving window and  $M$  is the length of the SE.

$$f_{ail}(n) = f(n) \oplus g(m) = \max \left\{ \begin{array}{l} f(n-m) + g(m), \\ 0 < n-m < N, 0 < m < M \end{array} \right\} \quad (1)$$

$$f_{ero}(n) = f(n) \ominus g(m) = \min \left\{ \begin{array}{l} f(n+m) - g(m), \\ 0 < n+m < N, 0 < m < M \end{array} \right\} \quad (2)$$

Based on (1) and (2)  $MMF_1$  can be established as defined by (3) aiming to extract the transient features of the signal.

$$MMF_1(n) = f_{ail}(n) - f_{ero}(n) \quad (3)$$

The length of numerical window in MM is dependent on  $M$ , which can be as short as two samples. The length of SE affects the sensitivity of fault detection, i.e. detection of the fault “pulses” [26]. In fact, most of the fault generated traveling waves present themselves as quasi-step signals. For this reason the SE used in this paper has a flat shape and its length  $M$  can be as short as 3.

The original MM does not have the function of polarity detection. Although such detection is possible and has been proposed in [16], it requires the signal to be processed by two quadratic SEs, which doubles the calculation burden. As an alternative, the authors observed that it is also possible to achieve the same goal with less computational burden by utilizing the apparent features of erosion and dilation waveforms. In Fig. 2, an 80 node step signal  $F(n)$  is processed by a flat SE ( $g(m) = [0,0,0]$ ). The  $MMF_1(n)$  using the traditional algorithm does not depict polarity characteristics. Nonetheless, it can be observed that the dilation signal lags the erosion signal when there is an ascending edge, and leads the erosion signal when there is a descending edge. This characteristic can be used to detect the signal polarity, as described by the mathematical functions (4) and (5), where  $\varepsilon$  is a small threshold close to zero for detecting the lag or lead feature ( $\varepsilon = 0.0001$ ).

$$\Delta f_{ero}(n) < \Delta f_{dil}(n) < -\varepsilon \\ MMF_2(n) = f_{ero}(n) - f_{dil}(n) \quad (4)$$

$$\Delta f_{dil}(n) > \Delta f_{ero}(n) > +\varepsilon \\ MMF_2(n) = f_{dil}(n) - f_{ero}(n) \quad (5)$$

The results of the modified method are presented together with those of a traditional MMF method and multi-level DWT method (with ‘db6’ as mother wavelet) in Fig. 2. It can be seen that the proposed method achieves the clearest and most accurate polarity detection. Moreover, the processing time for MMF based method has been verified to be 25%~30% faster than that for DWT method (based on Matlab simulation).

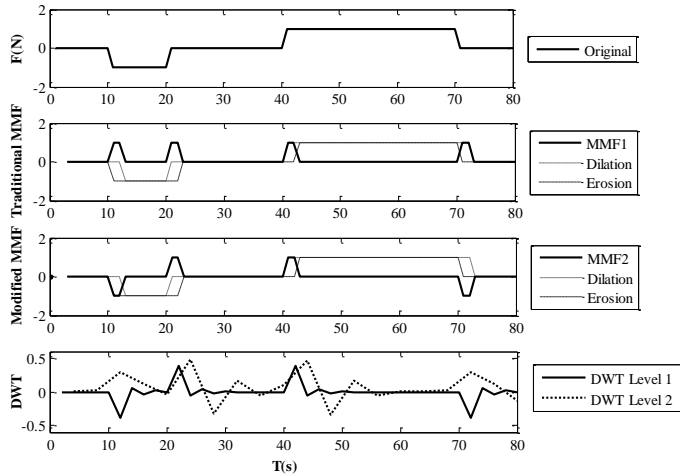


Fig. 2. MMF response comparison

### B. Noise reduction

Several denoising MMFs have been proposed in [26, 29] to deal with power system noise. However, before discussing the

denoising MMFs further, two other basic operators open (○) and close (●) need to be introduced:

$$f(n) \circ g(m) = (f(n) \ominus g(m)) \oplus g(m) \quad (6)$$

$$f(n) \bullet g(m) = (f(n) \oplus g(m)) \ominus g(m) \quad (7)$$

Open and close functions are used to smooth the positive impulses and negative impulses accordingly [30]. These functions are quite useful in noise reduction as the system noise is normally composed of a series of random impulses.

Based on the four operations introduced in (1), (2), (6) and (7), three major denoising MMFs, including *DEM*F (dilation and erosion median filter), *OCMF* (open and close median filter), *OCCOMF* (open-close and close-open median filter), are defined in (8), (9) and (10) respectively.

$$DEM(n) = (f(n) \oplus g(m) + f(n) \ominus g(m))/2 \quad (8)$$

$$OCMF(n) = (f(n) \circ g(m) + f(n) \bullet g(m))/2 \quad (9)$$

$$OCCOMF(n) = \\ \{f(n) \bullet [f(n) \circ g(m)] + f(n) \circ [f(n) \bullet g(m)]\}/2 \quad (10)$$

A comparison of these denoising MMFs conducted on a typical noisy fault current signal  $f(t)$  is presented in Fig. 3. The SNR level of the signal is 20dB. The length of SE ( $M$ ) is also considered as a variable in the test. It is found that both *OCMF* and *OCCOMF* methods are able to eliminate the majority of the noise and preserve the fault features at the same time, however, with clearer signal step change detection being achieved by *OCCOMF*. Therefore, *OCCOMF* with  $M=30$  is used in this paper. A short time delay (approximately 50  $\mu$ s) is considered insignificant in terms of protection system operation.

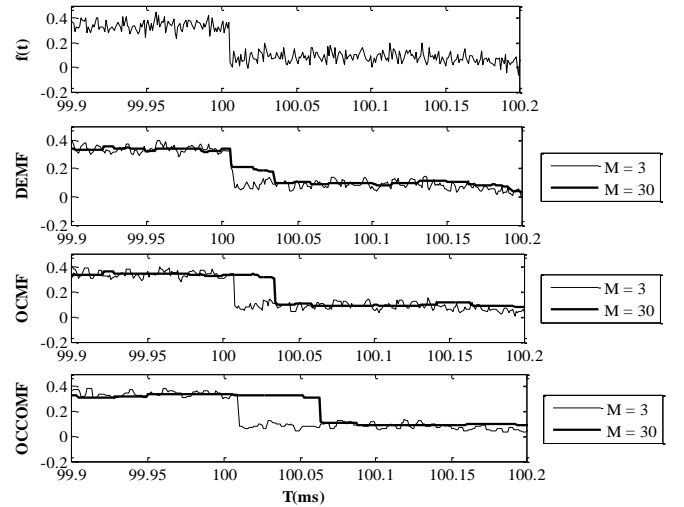


Fig. 3. Denoising performance comparison using MMFs.

### III. UNDERLYING PRINCIPLES OF THE PROPOSED SCHEME

The proposed MMF based scheme makes use of the traveling wave theory in electrical circuits. The traveling waves are usually illustrated in a Lattice diagram as shown in Fig. 4. In the

diagram, + and – define the polarity of the signal. In this section the application of two types of traveling wave based protection schemes is discussed, namely: single end method and double end method. The double end method is then extended to be the multi-end method for a meshed microgrid.

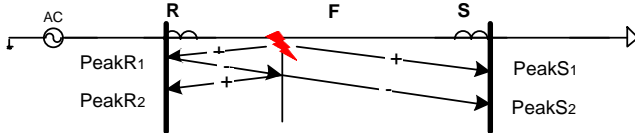


Fig. 4. Lattice diagram for a fault at F

#### A. Single end method

For single end method, extraction of two wavefronts to obtain their polarity and timing information are mandatory. At end R, the first two peak arrivals are time stamped as  $T_{peakR_1}$  and  $T_{peakR_2}$ . Their polarity information  $PpeakR_1$  and  $PpeakR_2$  are defined as: ‘1’ – positive and ‘–1’ – negative.

To discriminate the fault as ‘in zone’ or ‘out of zone’, fault location needs to be established. The calculation of fault location depends on whether the fault occurs in the first half of the line (Fig. 4) or in the second half of the line. For the former case, the second wavefront has the same polarity as the first one. For the latter case, it has the opposite polarity. The equations of fault location calculation are presented in (11), (12) and (13):

$$\Delta T_{peak} = T_{peakR_2} - T_{peakR_1} \quad (11)$$

$$\begin{aligned} PpeakR_1 \cdot PpeakR_2 &= 1 \\ \Rightarrow Distance &= \Delta T_{peak} \cdot v \end{aligned} \quad (12)$$

$$\begin{aligned} PpeakR_1 \cdot PpeakR_2 &= -1 \\ \Rightarrow Distance &= L - \Delta T_{peak} \cdot v \end{aligned} \quad (13)$$

where  $v$  is the speed of the traveling wave along the line,  $L$  is the length of the line, and  $T_{peak}$  and  $Ppeak$  present the time and polarity information of the traveling wavefront. However, single end method has the following inherent problems in microgrids:

- 1) The second wavefront is significantly damped by high resistive distribution lines.
- 2) The second wavefront can be cancelled out by the third wavefront or following wavefronts at specific fault locations, e.g. in the midpoint of the line.
- 3) To determine the fault position, the exact fault distance has to be calculated, which indicates that  $v$  along the line and the total line length need to be known.
- 4) If the line behind the relay and source impedance are considered, the algorithm becomes even more complicated. Hence, it is highly recommended to add a line trap to isolate the signals from behind.
- 5) The requirement of sampling accuracy and frequency is very high when the line length is short, which is a typical situation for most microgrids.

#### B. Double and multi-end method

For the double end method, units at both ends of a line need to only detect the initial wavefronts. It should be noted that the

initial polarity of the wavefront is always clear [24]. If the fault occurs in the protected line, the polarities of the first two wavefronts are the same; otherwise, the polarities are opposite. Based on this, the proposed fault indicator is defined as:

$$PpeakR_1 \cdot PpeakS_1 = 1 \quad (14)$$

It has been stated in [15] that, for a radial network, this indicator is sufficient. Additionally, there is no “Non-Detection Zone” caused by specific fault locations; close-up forward and close-up reverse faults can still be discriminated. To cater for a meshed network, the following additional indicator (15) is also proposed:

$$T_0 = \min \{T_0, T_1, T_2, T_3, \dots T_j\} \quad (15)$$

where  $T_0$  is the time arrival of the first wavefront at the local unit, and  $T_1, T_2, T_3, \dots T_j$  are the corresponding times obtained from the adjacent units. However, this indicator does not provide satisfactory performance in all meshed networks. One specific situation is a network with identical parallel lines, as illustrated in Fig. 5.

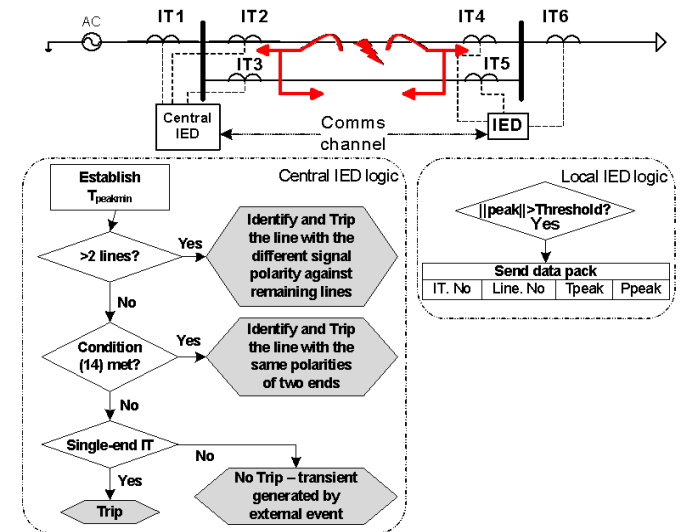


Fig. 5. Meshed network with parallel lines and the general protection scheme

This network has a pair of parallel lines equipped with IT2, IT4 and IT3, IT5. When a fault occurs in one of the parallel lines, the traveling wavefronts hit each other with the same polarity on the other parallel line; the instruments at the same bus share the same time information, which prevents proper discrimination of the fault location based on equation (15). Furthermore, for lines such as the one equipped with single-end instrument transformer IT 6, it further highlights the need for improvement in the protection strategy.

Therefore, in order to address these problems this paper introduces two additional elements to the protection logic to enhance the proposed MM based protection scheme:

- 1) For buses with more than two lines connected, the faulty circuit is identified from the wavefront polarity information as the faulty branch will always have opposite polarity with respect to the remaining circuits.

- 2) In cases where only two lines are in operation at the bus, as long as the upstream lines can be isolated to be within the healthy zone by taking the calculation in the equation (14), the single-end line is tripped instantaneously.

An updated protection strategy is presented Fig. 5. Each bus is set up with a local IED which detects any wavefront above a certain threshold and sends the relevant data (IT, circuit number, the time of first wavefront arrival and its polarity) to the central IED which subsequently evaluates which line is faulty and initiates the tripping signals to isolate the fault. Hence, reliable but relatively low bandwidth communications are required as only the time and polarity information within the network during the fault need to be transported.

#### IV. PERFORMANCE EVALUATION

For the evaluation of the performance of the proposed protection scheme PSCAD/EMTDC simulator is employed with a 20kV benchmark MV microgrid model [1] as illustrated in Fig. 6.

The simulation time step is 1 $\mu$ s. Four inverter-interfaced generators (IIG) are connected to buses 2, 4, 6 and 8 respectively, and two dynamic motor loads are connected to buses 3 and 7. The lines are 20kV ABB XPLE underground cables [31]. The power of IIGs is provided by the ideal DC sources, which sufficiently emulate the connected micro turbines and fuel cell systems, or any other source with storage on the DC side [32]. Each inverter is implemented with a mode-adaptive droop based dq-frame controller with detailed information presented in [33].

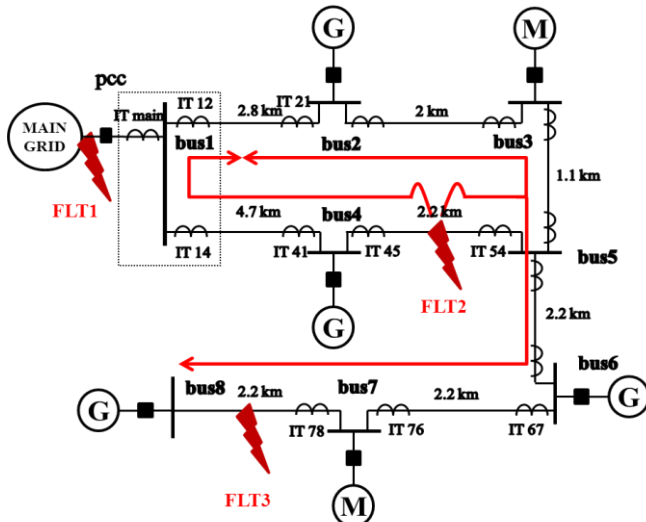


Fig. 6. Single line diagram of 20kV benchmark MV microgrid model

The overall protection scheme is firstly tested under three fault scenarios: FLT1, FLT2 and FLT3. A number of additional tests are subsequently performed to systematically assess the sensitivity and stability of the method under varying fault parameters.

##### A. Validation of the scheme under three fault scenarios

Three fault scenarios FLT1, FLT2 and FLT3 are simulated and the results of detected wavefront polarity as well as time

information are listed in Table I, with the earliest detection time and the critical signal polarities highlighted.

- 1) FLT1: an external fault at the grid near PCC during grid-connected operation;
- 2) FLT2: an internal fault inside a ring network that may cause traveling wavefronts hitting each other in healthy lines during islanded operation;
- 3) FLT3: an internal fault at a radial downstream line during islanded operation.

In scenario 1), considering the first additional logic element (introduced in section III.B), the fault is discriminated as external, since the signal of the main IT has the reversed polarity with respect to all other signals at Bus 1.

In scenario 2), there are two buses with the shortest arrival time. However, the faulty line is easily identified using equation (14).

In scenario 3) the fault is applied to a radial line with only single-end measurement. After distinguishing that the closest bus to the fault is Bus 7, the faulty line is recognized using the second additional logic element by ruling out the healthy adjacent lines.

TABLE I  
RESULTS USING MMF BASED PROTECTION SCHEME UNDER DIFFERENT FAULT SCENARIOS.

IT.	FLT1		FLT2		FLT3	
	Sign	Time (ms)	Sign	Time (ms)	Sign	Time (ms)
main	+	522.341	-	522.462	-	522.400
12	-	<b>522.341</b>	-	522.462	+	522.400
21	+	522.356	-	522.453	-	522.386
23	-	522.356	+	522.453	+	522.386
32	+	522.366	-	522.443	-	522.376
35	-	522.366	+	522.443	+	522.376
53	+	522.371	-	522.437	-	522.371
14	-	<b>522.341</b>	+	522.462	-	522.400
41	+	522.366	-	<b>522.437</b>	-	522.382
45	-	522.366	+	<b>522.437</b>	+	522.382
54	+	522.371	+	<b>522.437</b>	-	522.371
56	-	522.371	-	<b>522.437</b>	+	522.371
65	+	522.383	+	522.449	-	522.359
67	-	522.383	-	522.449	+	522.359
76	+	522.394	+	522.460	-	<b>522.347</b>
78	-	522.394	-	522.460	+	<b>522.347</b>

##### B. Impact of fault inception angle and fault resistance

In the proposed protection scheme, the signal peak is compared against a threshold and used as an initiating trigger for the data package sending to the central IED, as shown in Fig. 5. It is well known that the magnitude of the wavefront signal varies with the fault inception angle, line impedance and fault resistance. To investigate these effects, a fault is applied at the midpoint of the line 4-5 (FLT2 scenario), with fault impedance varying between 0.01 $\Omega$  and 50 $\Omega$  and point on wave (POW) of the fault inception between 0 ° and 90 °. The threshold is set to 0.01kA ( $\approx$ 20% of the rated current). However, it should be highlighted that in practice this threshold should be set appropriately to match the actual signal magnitude and noise levels as discussed in Section IV.E. The results indicate that the initial traveling wavefronts are all detectable with the POW as low as 5 ° regardless of the fault resistance (up to 50 $\Omega$ ).

Fig. 7 (islanded operation) and Fig. 8 (grid-connected operation) are two magnified sections of the graphs (i.e. POW

between  $0^\circ$  and  $5^\circ$ ) to help illustrate the dependence of the wavefront peak value at IT 45 on different fault inception angles and fault resistances. The blue plane stands for the threshold and white surface stands for the simulated peak value. Apparent close similarity of the two figures demonstrates the flexibility of the proposed scheme which is shown to be unaffected by the network mode of operation (islanded or grid connected).

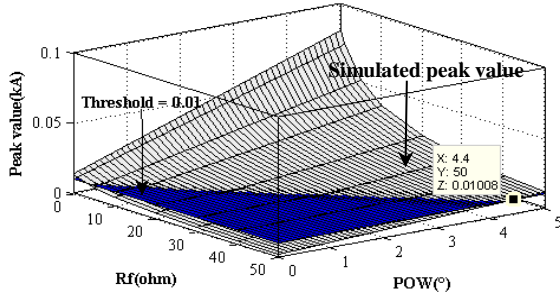


Fig. 7. Peak value of the traveling wavefront under different fault impedances and fault inception angles during islanded operation

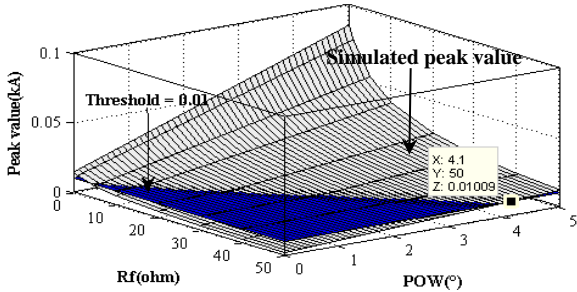


Fig. 8. Peak value of the traveling wavefront under different fault impedances and fault inception angles during grid connected operation.

### C. Impact of sampling frequency

The key element within the logic of the multi-end MMF based protection is time discrimination between the wavefronts arriving at different units. This is closely related to the sampling frequency, the speed of traveling wave, and distance (cable length) between the units. Knowing the parameters of the cable, the speed of the traveling wave  $v$  can be obtained. The requirement for the largest sampling time step  $T_s$  as a function of distance  $D$  between two units is presented in (16).

$$T_s = \frac{1}{f_s} < \frac{k_c}{f_c} = k_c T_c = \frac{k_c D}{v} \quad (16)$$

where  $f_s$  is the sampling frequency,  $T_c$  is the traveling time along the cable, and  $k_c$  is the safety factor ranging from 0.5~0.9 to ensure time discrimination of wavefront arrivals between two ends of a shortest line.

To illustrate this, a solid fault with POW of  $90^\circ$  is applied to line 4-5 (FLT2 in Fig. 6), while IT 14 and IT 45 are monitored with reduced length of line 1-4 (0.5km) and two different sampling frequencies. The microgrid is running in islanded mode of operation. To prevent the healthy zone (in this case bus 1 and bus 2) from being disconnected, it is necessary to detect a time difference between bus 1 and bus 4. Fig. 9. presents the initial wavefronts from unit 1 and unit 4 when the cable length between them is 0.5km. As can be seen, at sampling frequency

of 0.2MHz, it is impossible to detect the time difference. According to formula (16) the sampling frequency need to be at least  $f_s = \frac{v}{k_c D} = \frac{2.25e5}{0.8 \times 0.5} = 0.56\text{MHz}$ .

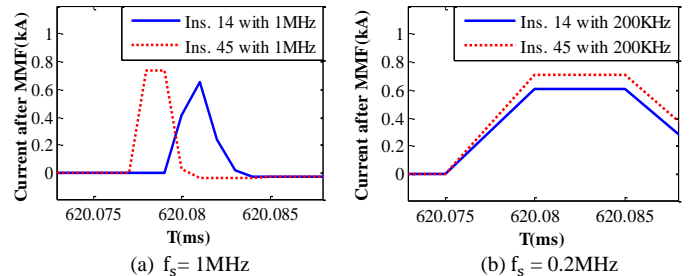


Fig. 9. Time deviation of extracted initial wavefronts from units 1 and 4 under different sampling frequencies

### D. Stability under transient disturbances

The test results under selected worst case scenarios are presented in Fig. 10. The indicators shown in the figure are chosen from the phase with the highest magnitude. The non-fault disturbances in the microgrid include events such as: motor-starting (a); transients during mode of operation transfer (b) and (c); and change of system topology (d). As shown in Fig. 10, with applied threshold of 0.01kA, the MMF based main protection scheme presents no detectable response to these transients. Hence it can be concluded that the proposed scheme shows good stability in response to all simulated non-fault disturbances.

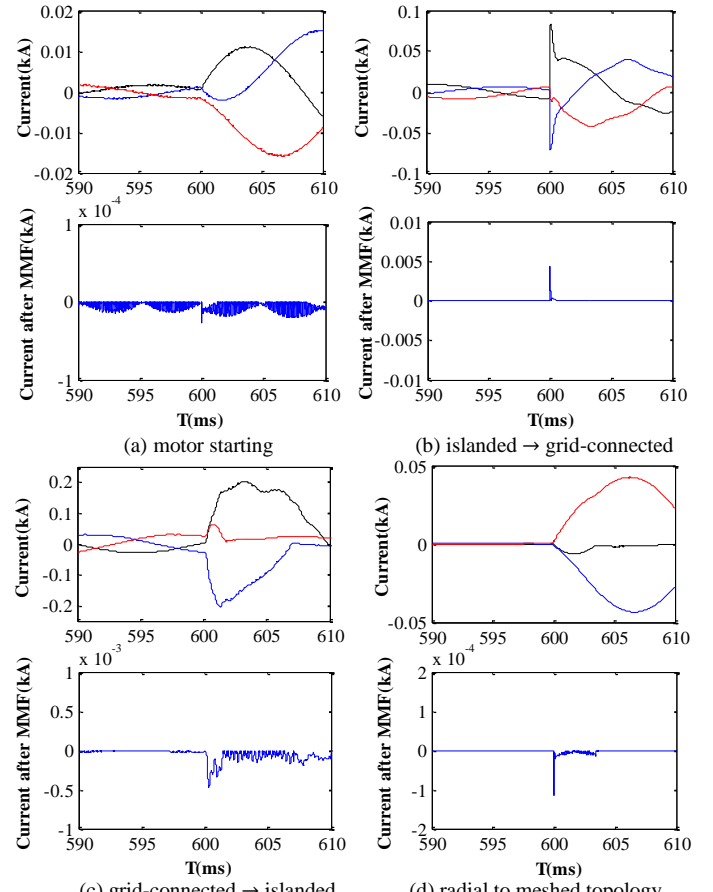


Fig. 10. The responses of MMF based protection scheme to non-fault system disturbances

### E. Impact of noise level

The impact of noise level on the protection sensitivity is evaluated by contaminating the fault current from IT 45 under FLT 2 scenario with white noise (SNR ranges from 40dB to 10dB).

The results are presented in Fig. 11 and Fig. 12. It can be seen that the noisy signal with SNR down to 10dB can still be successfully processed with clear wavefront polarity and time location. However, this would require slightly higher sensitivity threshold for peak detection, which might become problematic when the fault occurs with a very low fault inception angle, as shown in Fig. 12(d). A search through a short window for the maxima modulus of the indicator is one of the solutions to solve this problem. The threshold of the peak detection is then lifted up by increased noise level. Normally as far as the feature of the initial wavefronts has not been overpowered by the noise, the transient feature can be extracted correctly.

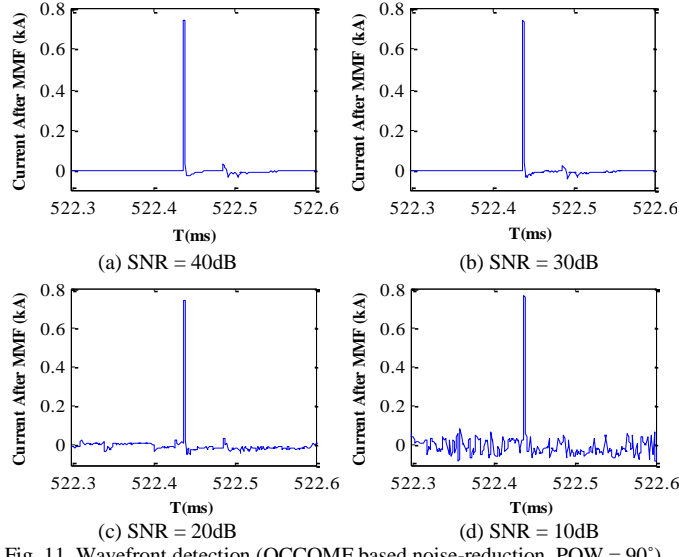


Fig. 11. Wavefront detection (OCCOMF based noise-reduction, POW = 90°)

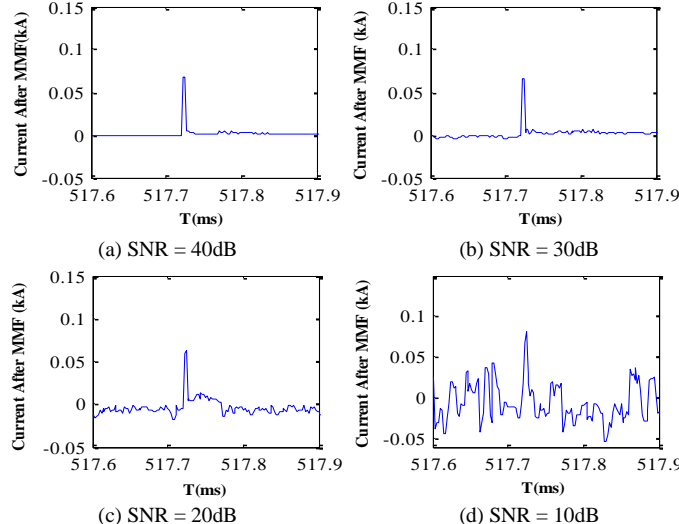


Fig. 12. Wavefront detection (OCCOMF based noise-reduction, POW = 5°)

### V. POTENTIAL HARDWARE IMPLEMENTATION

Although traveling wave methods have been proposed for high voltage transmission system protection for more than 20 years, the practical implementation has been inhibited mainly by the limitations of signal processing hardware. An MM based signal processing algorithm, which only contains addition and subtraction operations within a numerical window of 3~12 samples, significantly lightens the signal processing burden. Besides, this protection scheme is only activated when a traveling wavefront is detected in the microgrid. Only time and polarity of initial traveling wavefronts need to be communicated. Furthermore, communication channels are becoming increasingly more common in distribution grids and can satisfy very moderate bandwidth requirements of the proposed protection scheme.

Despite many obvious advantages, high frequency sampling and accurate signal synchronization are still needed. As discussed in section IV.C, the sampling frequency for the MV benchmark microgrid needs to be in excess of 256kHz ( $f_s = \frac{v}{k_c D} = \frac{2.25e5}{0.8 \times 1.1} \approx 256\text{kHz}$ ), which can be considered achievable by modern acquisition hardware. GPS based synchronization is taken into account in this paper, although a cheaper alternative such as the ping-pong algorithm may also be applied [34]. The errors in latency estimation can be compensated by scaling the safety factor  $k_c$ , which will be studied in the future.

Additionally, Rogowski coil or Hall Effect based current instruments should be considered as they are capable of covering wide frequency bandwidth, and are typically used in traveling wave applications. Hi-pass filters should be used to remove low frequency components and sample-and-hold elements to maintain synchronous sampling of all phases.

### VI. CONCLUSION

Considering the trends in the distribution systems and microgrids, this paper proposes a Mathematical Morphology based multi-end protection scheme using initial current traveling wavefronts as a main fault detection mechanism. The method uses both time and polarity information of the traveling waves with moderate communication requirements, delivering dependable and secure performance under different system topologies and modes of operation. The paper provides a mathematical description of a modified MMF with polarity detection built on the apparent features of erosion and dilation waveforms. The further proposed two new logics help establish a systematic protection scheme for varied system topologies and configurations including meshed networks with parallel lines and remote feeders with single-end measurement. Using transient simulation in PSCAD/EMTDC, the new protection scheme has been proven to be able to accurately locate the fault with POW as low as 5° regardless of the fault resistances and system fault level. It is also confirmed to be an effective method under noisy condition. Moreover, the stability of the proposed scheme has been verified under non-fault disturbances such as motor starting, operational mode transfer and topology changes. Hardware requirements of the scheme have been considered as

economically viable and future work will concentrate on the development of a hardware laboratory prototype. It is to be noted that some special fault conditions such as switch on fault and simultaneous multi-located faults, and the impact from the earthing arrangement, also need to be considered in future research.

## REFERENCES

- [1] N. El Halabi, M. Garc ía-Gracia and J. Borroy et al., "Current Phase Comparison Pilot Scheme for Distributed Generation Networks Protection," *Applied Energy*, vol. 88, no. 12, pp. 4563–4569, Dec. 2011.
- [2] A. R. Haron, A. Mohamed and H. Shareef, "A Review on Protection Schemes and Coordination Techniques in Microgrid System," *J. of Appl. Sciences*, vol. 12, no. 2, pp. 101–112, Feb. 2012.
- [3] H. Nikkhajoei and R. H. Lasseter, "Microgrid Protection," in *IEEE Power Eng. Soc. General Meeting*, 2007, pp. 1–6.
- [4] F. Van Overbeeke, "Fault Current Source to Ensure the Fault Level in Inverter-Dominated Networks," in *20th Int. Conf. And Exhibition On Electricity Distribution - Part 1, CIRED*, 2009, pp. 1–4.
- [5] X. Tan, Q. Li, and H. Wang, "Advances and Trends of Energy Storage Technology in Microgrid," *Int. J. of Elect. Power & Energy Syst.*, vol. 44, no. 1, pp. 179–191, Jan. 2013.
- [6] H. Al-Nasseri, M. A. Redfern and R. O'gorman, "Protecting Micro-grid Systems Containing Solid-State Converter Generation," in *2005 Int. Conf. on Future Power Syst.*, 2005, pp.1–5.
- [7] H. Al-Nasseri and M. A. Redfern, "Harmonics Content Based Protection Scheme for Micro-Grids Dominated by Solid State Converters," in *Power System Conf., 12th Int. Middle-East, Mepcon*, 2008, pp. 50–56.
- [8] W. Jiang, Z. He and Z. Q. Bo, "The Overview of Research on Microgrid Protection Development," in *Proc. ISDEA*, 2010, vol. 2, pp. 692–697.
- [9] H. H. Zeineldin, E. F. El-Saadany and M. M. Salama, "Distributed Generation Micro-Grid Operation: Control and Protection," in *Power Syst. Conf.: Advanced Metering, Protection, Control, Communication, and Distributed Resources, Ps '06*, 2006, pp. 105–111.
- [10] M. Dewadasa, A. Ghosh and G. Ledwich, "Protection of Microgrids Using Differential Relays," in *Proc. AUPEC, Australasian*, 2011, pp. 1–6.
- [11] E. Sortomme, S. S. Venkata and J. Mitra, "Microgrid Protection Using Communication-assisted Digital Relays," *IEEE Trans. Power Del.*, vol. 25, no. 4, pp. 2789–2796, Oct. 2010.
- [12] M. Dewadasa, A. Ghosh and G. F. Ledwich, "Distance Protection Solution for a Converter Controlled Microgrid," *Faculty of Built Environment And Eng.; School of Eng. Syst.*, 18-Dec-2008. [Online]. Available: <http://www.ee.iitb.ac.in/~npsc2008/>.
- [13] T. David, S. Mark, C. David and C. Ed et al., "DC Power System Fault Protection - Test of Novel Techniques," in *Engine As a Weapon*, Portsmouth Historic Dockyard, UK, 2009.
- [14] S. Shi, B. Jiang, X. Dong and Z. Bo, "Protection of Microgrid," in *Proc. IET DPSP*, 2010, pp. 1–4.
- [15] X. Li, A. Dyško and G. Burt, "Enhanced Protection for Inverter Dominated Microgrid Using Transient Fault Information," in *Proc. IET DPSP*, Birmingham, UK, 2012, pp. 1–5.
- [16] Q. H. Wu, J. F. Zhang and D. J. Zhang, "Ultra-High-Speed Directional Protection of Transmission Lines Using Mathematical Morphology," *IEEE Trans. Power Del.*, vol. 18, no. 4, pp. 1127– 1133, Oct. 2003.
- [17] L. Zou, P. Liu and Q. Zhao, "Mathematical Morphology Based Phase Selection Scheme in Digital Relaying," *Generation, Transmission And Distribution, IEE Proc.*, vol. 152, no. 2, pp. 157– 163, Mar. 2005.
- [18] F. H. Magnago and A. Abur, "Fault Location Using Wavelets," *IEEE Trans. On Power Del.*, vol. 13, no. 4, pp. 1475–1480, Oct. 1998.
- [19] C. Aguilera, E. Orduna and G. Ratta, "Directional Traveling-Wave Protection Based on Slope Change Analysis," *IEEE Trans. Power Del.*, vol. 22, no. 4, pp. 2025–2033, Oct. 2007.
- [20] X. Chen, Z. Xu and J. Suo, "Bandpass Filter Design Based on Wavelet Packet," in *Proc. IASP*, 2010, pp. 75–78.
- [21] W. Chen, O. P. Malik and X. Yin et al., "Study of Wavelet-Based Ultra High Speed Directional Transmission Line Protection," *IEEE Trans. Power Del.*, vol. 18, no. 4, pp. 1134– 1139, Oct. 2003.
- [22] X. Dong, Y. Ge and J. He, "Surge Impedance Relay," *IEEE Trans. Power Del.*, vol. 20, no. 2, pp. 1247– 1256, Apr. 2005.
- [23] P. Jafarian and M. Sanaye-Pasand, "A Traveling-Wave-Based Protection Technique Using Wavelet/Pca Analysis," *IEEE Trans. Power Del.*, vol. 25, no. 2, pp. 588–599, Apr. 2010.
- [24] X. Dong, W. Kong and T. Cui, "Fault Classification and Faulted-Phase Selection Based on the Initial Current Traveling Wave," *IEEE Trans. Power Del.*, vol. 24, no. 2, pp. 552–559, Apr. 2009.
- [25] I. W. Selesnick, R. G. Baraniuk, and N. C. Kingsbury, "The Dual-tree Complex Wavelet Transform," *IEEE Signal Process. Mag.*, vol. 22, no. 6, pp. 123–151, Nov. 2005.
- [26] S. Gautam and S. M. Brahma, "Overview of Mathematical Morphology in Power Systems — a Tutorial Approach," in *IEEE Power & Energy Soc. General Meeting, 2009. Pes '09*, 2009, pp. 1–7.
- [27] S. K. Buggaveeti and S. M. Brahma, "Improved Overcurrent Protection of Capacitor Banks Using Mathematical Morphology," *IEEE Trans. Power Del.*, vol. 26, no. 3, pp. 1972–1979, Jul. 2011.
- [28] H. J. A. M. Heijmans, *Morphological Image Operators*. Academic Press, 1994.
- [29] W. Zhang, X. Zhou and Y. Lin, "Application of Morphological Filter in Pulse Noise Removing of Vibration Signal," in *Congr. on Image and Signal Process., 2008. Cisp '08*, 2008, vol. 1, pp. 132–135.
- [30] L. Zhang, J. Xu, J. Yang and D. Yang, "Multiscale Morphology Analysis and Its Application to Fault Diagnosis," *Mech. Syst. and Signal Process.*, vol. 22, no. 3, pp. 597–610, Apr. 2008.
- [31] ABB, *Abb XLPE Cable Guide Rev. 1*, 2005. [Online]. Available: <http://www.scribd.com/doc/36172955/XLPE-Cable-Systems-Users-Guide>.
- [32] P. Piagi and R. H. Lasseter, "Autonomous Control of Microgrids," in *IEEE Power Eng. Soc. General Meeting, 2006*.
- [33] X. Li, A. Dyško and G. Burt, "Enhanced Mode Adaptive Decentralized Controller for Inverters Supplying a Multi-bus Microgrid," in *Proc. IEEE ISGT Europe, Copenhagen, Denmark*, 2013.
- [34] D. Xie and J. Peng, "An Research of Ping-Pong Clock Synchronization Based on Quantum Optics," in *Proc. SOPO*, 2010, pp. 1 –4.



**Xinyao Li** (S'10) received the B.Sc. degree from Hohai University of Nanjing, China, in 2008. Then she worked for Nanjing Nari-relays Electric Co., China, from 2008 to 2009. She is pursuing the Ph.D. degree within the Institute for Energy and Environment at the University of Strathclyde, Glasgow, U.K.

Currently she is a Research Associate at the University of Strathclyde. Her current research interests are power system protection and control.



**Adam Dyško** (M'06) received the M.Sc. degree from the Technical University of Łódź, Poland, in 1990, and the Ph.D. degree from the University of Strathclyde, Glasgow, U.K., in 1998.

Currently, he is a Lecturer in the Department of Electronic and Electrical Engineering, University of Strathclyde. His research interests include power system modeling and simulation, power system protection, and power quality.



**Graeme M. Burt** (M'95) received the B. Eng. degree in electrical and electronic engineering from the University of Strathclyde, Glasgow, U. K., in 1988 and the Ph.D. degree from the University of Strathclyde in 1992. He is currently a Professor within the Institute for Energy and Environment at the University of Strathclyde.

He is currently the Director of the University Technology Centre in Electrical Power Systems sponsored by Rolls-Royce and is a Director of the Institute for Energy and Environment.